How to cite: Angew. Chem. Int. Ed. 2024, e202319010
doi.org/10.1002/anie.202319010

Zinc Batteries | Very Important Paper

For Zinc Metal Batteries, How Many Electrons go to Hydrogen Evolution? An Electrochemical Mass Spectrometry Study

Kingshuk Roy[+], Ashutosh Rana[+], Joseph N. Heil[+], Brian M. Tackett, and Jeffrey E. Dick**

Abstract: Despite the advantages of aqueous zinc (Zn) metal batteries (AZMB) like high specific capacity (820 mAh g^{-1} and 5,854 mAh cm^{-3}), low redox potential (−0.76 V vs. the standard hydrogen electrode), low cost, water compatibility, and safety, the development of practically relevant batteries is plagued by several issues like unwanted hydrogen evolution reaction (HER), corrosion of Zn substrate (insulating ZnO, $Zn(OH)_2$, $Zn(SO_4)_x(OH)_y$, $Zn(ClO_4)_x(OH)_y$ etc. passivation layer), and dendrite growth. Controlling and suppressing HER activity strongly correlates with the long-term cyclability of AZMBs. Therefore, a precise quantitative technique is needed to monitor the real-time dynamics of hydrogen evolution during Zn electrodeposition. In this study, we quantify hydrogen evolution using in situ electrochemical mass spectrometry (ECMS). This methodology enables us to determine a correction factor for the faradaic efficiency of this system with unmatched precision. For instance, during the electrodeposition of zinc on a copper substrate at a current density of 1.5 mA/cm^2 for 600 seconds, 0.3 % of the total charge is attributed to HER, while the rest contributes to zinc electrodeposition. At first glance, this may seem like a small fraction, but it can be detrimental to the long-term cycling performance of AZMBs. Furthermore, our results provide insights into the correlation between HER and the porous morphology of the electrodeposited zinc, unravelling the presence of trapped H_2 and Zn corrosion during the charging process. Overall, this study sets a platform to accurately determine the faradaic efficiency of Zn electrodeposition and provides a powerful tool for evaluating electrolyte additives, salts, and electrode modifications aimed at enhancing long-term stability and suppressing the HER in aqueous Zn batteries.

Introduction

Aqueous Zinc-metal battery chemistry has garnered recent attention due to several favorable properties of zinc metal such as high specific capacity (820 mAh g^{-1} and 5,854 mAh cm^{-3}), a low redox potential (−0.76 V vs. the standard hydrogen electrode), innate compatibility with aqueous electrolytes, low cost, and safety.[1–5] The commonly used electrolytes for reversible AZMBs are mildly acidic in nature (pH: 4–6).[4,6–9] However, the commercialization of Zn-metal battery chemistry faces several challenges. These challenges include issues such as the unwanted hydrogen evolution reaction (HER) and dendritic growth during the charging process. These drawbacks can exacerbate other parasitic reactions, ultimately leading to the formation of a ZnO passivation film along with other passivation products like $Zn(OH)_2$, $Zn(SO_4)_x(OH)_y$, $Zn(ClO_4)_x(OH)_y$ etc., which are insulating by nature, and their presence can increase the overall cell resistance, which is detrimental to the long-term cyclability of AZMBs.[10–15] These drawbacks are often interrelated and can trigger one another. However, it is essential to recognize that the issues mentioned earlier primarily pertain to the Zn anode. The cathode poses an entirely different set of challenges, which is not the primary focus of this work.

Among all the previously mentioned issues, HER during the charging of AZMBs appears to be of paramount importance. Several studies have demonstrated that controlling and suppressing HER can significantly enhance the performance of AZMBs.[16–23] In a typical zinc-ion electrolyte, Zn^{2+} forms octahedral $[Zn(H_2O)_6]^{2+}$ complexes, where solvent (H_2O) molecules can coordinate with the Zn^{2+} center, resulting in the creation of "solvated water." Within the electrolyte bulk, besides solvated water, there are also free water molecules that do not participate in any coordination activities with Zn^{2+}. Various studies have demonstrated that HER during the charging process is influenced by both the Zn^{2+} solvation structure and the H-bond network of free water.[4] However, there is limited understanding regarding the relative contributions of solvated and free water molecules to the overall hydrogen liberation in the system. Several strategies are employed to

[*] K. Roy,[+] A. Rana,[+] J. E. Dick
Department of Chemistry, Purdue University
West Lafayette, IN 47907 (USA)
E-mail: jdick@purdue.edu
J. N. Heil,[+] B. M. Tackett
Davidson School of Chemical Engineering, Purdue University
West Lafayette, IN 47907 (USA)
E-mail: bmtacket@purdue.edu
J. E. Dick
Elmore Family School of Electrical and Computer Engineering, Purdue University
West Lafayette, IN 47907 (USA)
[+] These authors contributed equally to this work.

control the HER and achieve long-term cyclability in AZMBs. These strategies include the regulation of electrolyte composition and structure, the addition of electrolyte additives, cosolvents, etc.[24–28,45–47] For instance, a concentrated aqueous electrolyte with specific salts has been devised to reduce solvated water and inhibit HER.[29] Conversely, an alternative approach focuses on minimizing the activity of free water by incorporating additives that disrupt the hydrogen bond network of free water.[30] Therefore, we believe that a quantitative approach to monitoring and understanding HER is crucial for the development of commercially relevant zinc battery chemistries. Few studies have delved into the understanding and quantification of HER during the charging process (electrodeposition of zinc) in AZMBs.[31–33] Many studies in the literature predominantly employ gas chromatography (GC) to understand and quantify HER. However, GC is not the ideal technique to quantify evolved H_2.[31–33] The intrinsic delay associated with GC measurements generally means this technique is unable to resolve differences in H_2 flux within the charging time interval, making it impossible to track changes in HER dynamics over the course of the deposition process. Further, GC suffers from poor sensitivity and precision when measuring the low concentrations of hydrogen present in an electrolyte following deposition. As far as our current knowledge extends, there have been no studies to date capable of promptly and precisely quantifying the extent of the HER during the charging process of AZMBs.

In this study, we introduce, for the very first time, a methodology that utilizes in situ electrochemical mass spectrometry (ECMS) to provide an accurate and real-time measurement of the HER during the electrodeposition of zinc, marking to the best of our knowledge the first battery-focused application of this system. By calibrating the mass spectrometer, we enable the quantification of H_2 generated during the application of voltage or current biases. The geometry of the ECMS setup allows for 100 % collection of volatile products generated at the working electrode, providing exceptional sensitivity.[34] Notably, the desorption of less than one monolayer of hydrogen equivalents on planar electrodes can be accurately quantified by this technique. The design of the system is such that volatile species produced are detected by the mass spectrometer within seconds, providing much better time resolution compared to GC.[34] This platform enables precise quantification of HER during galvanostatic zinc plating, thus enabling accurate Zn electrodeposition faradaic efficiency calculations and offering insights into the correlation between HER and the porous morphology of the deposited zinc.

Results and Discussion

As previously demonstrated, AZMB chemistry in mildly acidic electrolytes is afflicted by several drawbacks including non-uniform dendritic growth, which can result in short circuits, passivation leading to the formation of an insulating zinc oxide film which in turn triggers increase in cell potential, and the occurrence of the hydrogen evolution reaction during the electrodeposition of zinc.[12,13,15,17,19,35] It is essential to note that these drawbacks are intricately interconnected and collectively contribute to the deterioration of AZMB performance during extended cycling studies. First, this study discusses and explores the nature of these drawbacks. Subsequently, electrochemical mass spectroscopy as a platform for monitoring the real-time evolution of hydrogen during electrodeposition is showcased.

Linear sweep voltammetry with time-synchronised optical microscopy was performed in a three- electrode setup wherein, a 1 mm dia. Cu disk electrode was used as the working electrode, zinc foil as the counter electrode, and Ag/AgCl in 1 M KCl as the reference electrode in 0.5 M $ZnSO_4$ electrolyte. LSV was performed at between an initial potential of −0.8 V to a final potential of −1.6 V at a scan rate of 10 mV/s, resulting in a voltammogram shown in Figure 1(a). Along with scanning the potential at the Cu disk, bright field optical micrographs were simultaneously acquired to monitor the nature of electrodeposited zinc and observe HER activity at the Cu|electrolyte interface. During the initial segment of the sweep (−0.8 V to −1 V), no redox activity was observed, as depicted by micrograph (1) in Figure 1(b). It was only when we swept to a more negative potential, surpassing the nucleation barrier at −1.04 V vs Ag/AgCl for Zn deposition on the Cu substrate, that we observed an exponential rise in current (highlighted in the orange region in Figure 1(a)). Initially, as predicted by Butler–Volmer electron transfer kinetics, we observe an exponential increase in current in this portion, representing a charge transfer-controlled regime. During this segment, we observe nucleation of zinc clusters evident from micrograph (2) shown in Figure 1(b), although no HER activity is observed. However, as we continue to sweep to more negative potentials, we observe the growth of deposited Zn clusters, as depicted by micrograph (3) in Figure 1(b), accompanied by substantial HER activity. As shown by the yellow region in Figure 1(a), there is a significant surge in current, leading to a steady-state-like condition as the system transitions from an initial charge transfer-controlled regime to a diffusion-limited regime. There is a transition in the reaction mechanism from charge transfer control to diffusion control due to the consumption of Zn^{2+} ions in the vicinity of the electrode surface. This consumption induces a form of diffusion limitation, where the rate-limiting step shifts from the kinetics of electron transfer to the diffusion of Zn^{2+} ions to the electrode surface, a phenomenon commonly referred to as diffusion control. It is well established in the literature that a diffusion limitation during electrodeposition is closely associated with dendrite formation. Figure S1 illustrates the impact of transitioning between reaction regimes, specifically from charge transfer control to diffusion control, on the morphology of electrodeposited zinc. This mechanism is not only applicable to zinc electrodeposition but also holds true for other metal battery chemistries involving the use of Na and Li. It is often cited in the literature to explain the origin of dendrite formation during electrodeposition. Furthermore, the overall current escalation is also related to the increasing

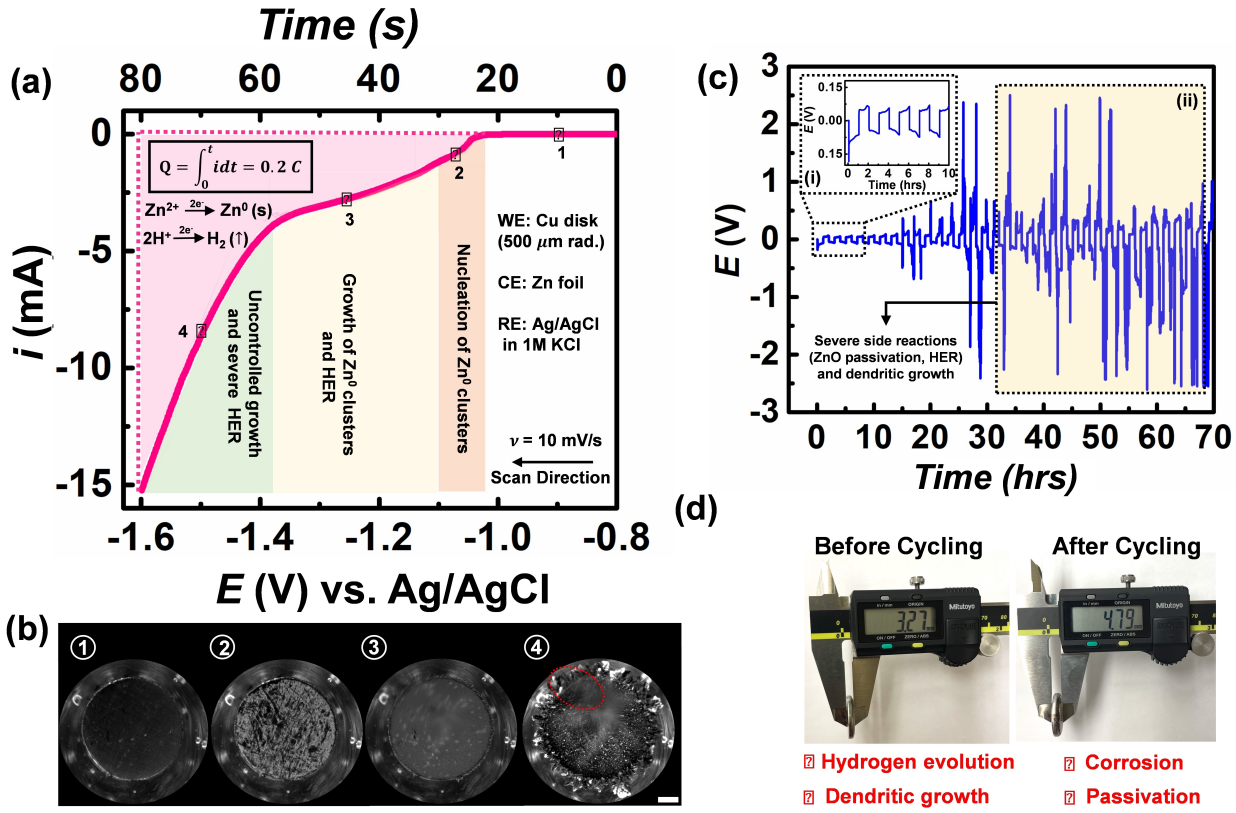

Figure 1. (a) Linear sweep voltammogram for the electrodeposition of zinc on the custom-made Cu electrode (1 mm diameter) using aqueous Aq. 0.5 M $ZnSO_4$ as the electrolyte; (b) Time-synchronized bright-field optical microscopy images for the electrodeposited Zn on Cu as a function of time/voltage (1, 2, 3, and 4 are the images captured at different times, and the corresponding potential is depicted in Figure 1(a). (c) Voltage vs. time trace for cycling of a zinc-symmetric cell galvanostatically charged and discharged at a current of 1 mA/cm^2 with a capacity of 1 mAh/cm^2 (d) Measurements for the coin cell thickness before and after cycling showed severe swelling of the cell, indicating a severe hydrogen evolution reaction, corrosion, and non-uniform dendritic growth.

electroactive surface area of the electrode. Succeeding the −1.38 V threshold results in a dramatic increase in the value of current (the green region in Figure 1(a)) due to the uncontrolled zinc growth (dendrites) and heightened HER activity, as shown in micrograph (4) in Figure 1(b).

It is well established in the literature that a diffusion limitation during electrodeposition is closely associated with dendrite formation.[36,37] Furthermore, the overall current escalation is also related to the increasing electroactive surface area of the electrode. Succeeding the −1.38 V threshold results in a dramatic increase in the value of current (the green region in Figure 1(a)) due to the uncontrolled zinc growth (dendrites) and heightened HER activity, as shown in micrograph (4) in Figure 1(b). A closer look at the micrograph reveals a substantial HER activity at the electrode surface (dashed red circle). A time-synchronized video in the Supporting Information (Movie S1) shows the side-by-side morphological evolution of the electrode surface and the voltametric response.

One might wonder about the influence of scan rate on the nature of voltammograms and the morphology of electrodeposited zinc. To explore this, Figure S2 presents voltammetry experiments under the same experimental conditions as depicted in Figure 1(a), but with varying scan rates (0.5 mV/s, 1 mV/s, 5 mV/s, 10 mV/s, and 20 mV/s). Significant differences in the magnitude of current have been observed across these various scan rates. The slowest scan rate specifically resulted in the smallest magnitude of observed current, while the observed current increased with higher scan rates. This change in the magnitude of current transients further suggests differences in the morphology of the electrodeposited zinc. However, upon closer examination of the voltammograms, the characteristics of the voltammogram's nature at various scan rates seem similar across multiple scan rates. Colored regions like 2, 3, and 4 in Figure 1(a) can be identified consistently for all cases.

It is to be noted that during the electrodeposition of zinc in the voltammetry experiment, it is not possible to precisely assign exact regions to initial nucleation (charge-transfer control) and growth (diffusion control) as these are intrinsically convoluted with one another. Therefore, the color-coded regions (2, 3, and 4) in Figure 1(a) only serve as a qualitative illustration to demonstrate the transition in the rate-limiting step of the electrodeposition reaction from an initial charge transfer control (nucleation) to diffusion control (growth of Zn^0 clusters).

Overall, this clearly shows that Zn electrodeposition is closely associated with the formation of dendrites and HER. Along with voltage as the x-axis, a time axis is provided which shows the time points at which the potentials were applied. The charge (Q) passed during the voltage sweep was calculated by integrating the area under the current-time trace, as shown the pink region in Figure 1(a). The value of Q was found to be 0.2 C, which includes contributions from two different reduction reactions: conversion of Zn^{2+} to Zn^0 clusters and H_2O/H^+ to evolved H_2. This raises a fundamental question about the faradaic efficiency of the system: Can the contributions of these distinct reduction reactions be deconvoluted?

In practical applications of AZMBs, voltage sweeps are eschewed as a bias for zinc electrodeposition on the current collector. Instead, chronopotentiometry, involving the application of a constant current for a fixed time, is employed. To illustrate the issues associated with zinc electrodeposition, zinc symmetric cells were fabricated using the same electrolyte (0.5 M $ZnSO_4$) as the oltametric experiments. The cells were galvanostatically charged and discharged at a current of 1 mA/cm^2 with a capacity of 1 mAh/cm^2. The voltage vs. time profile is shown in Figure 1©. Initially, a stable voltage vs. time profile was observed (inset (i) of Figure 1 < xfig©-(c)), but beyond 15 hours, severe voltage fluctuations emerged, reaching as high as ±2.5 V, which is detrimental for long-term coin cell stability. During the cycling of the coin cells, we observed fluctuations in the voltage profile, indicating unstable cycling of the coin cell, wherein the voltage window increased from ±150 mV to ±2.5 V after 20 hours of cycling. These fluctuations arise from the changing morphology of electrodeposited zinc, HER, and formation of passivating side products that are insulating in nature. Such fluctuations are indicative of poor cycling performance and are detrimental to the cycle life of batteries, currently a key limitation in zinc metal batteries. $ZnSO_4$ being used as the electrolyte, The insulating passivating film mostly consists of $Zn_4SO_4(OH)_6$. xH_2O (ZSOH).[24] An XRD data of the passivation product formed can be found in the Supporting Information (Figure S3). It has been reported in literature that nature of zinc deposits can be porous because of HER, which can lead to an irreversible loss of capacity with cycling due to formation of dead zi.[38–41] This behaviour was consistently observed across multiple coin-cell experiments. The formation of dendrites during zinc electrodeposition can be detrimental to the long-term cyclability of zinc metal batteries and is often related to the formation of dead zinc, leading to irreversible capacity loss. Movie S2 shows the stripping of the electrodeposited zinc ioltametricmetric experiment shown in Figure 1(a) at a fixed potential of −0.6 V, where it can clearly be seen that dead zinc is formed as the dendrites slowly detach from the surface. Furthermore, the effect of HER is evident in the cell's thickness (as shown in Figure 1(d)), increasing from 3.27 mm before cycling to 4.79 mm after 70 hours of cycling, posing serious safety concerns. Overall, this underscores the importance of accurately quantifying the extent of HER during zinc cycling for a comprehensive understanding of the failure mechanisms in coin cells. In a broader context, the real-time quantification of HER during cycling serves as a valuable tool for the evaluation of electrolyte additives, electrolyte salts, or electrode modifications aimed at mitigating any undesirable side reactions and achieving prolonged stability in coin cells.

In the following discussion, we introduce electrochemical mass spectroscopy (ECMS) as a method for real-time quantification of the HER activity during zinc electrodeposition. In our experiments, we utilized helium (with a research purity of 6N, obtained from A-OX Welding) delivered via an internal mass flow controller. This carrier gas is responsible for maintaining the pressure gradient, facilitating the convection of gaseous species into the mass spectrometer (MS) inlet. The working electrode was composed of a copper (Cu) disk, and the reference electrode was Ag/AgCl immersed in 3.4 M KCl (supplied by eDAQ), with a platinum (Pt) wire serving as the counter electrode. These electrodes were connected to a potentiostat (Biologic SP-300) under the control of EC-Lab software. The Zilien software (from Spectro Inlets) was employed to manage the valves, mass spectrometer, and data collection. Data processing was conducted using the ixdat Python package, specifically developed for the analysis of ECMS. A detailed schematic, methodology, and H_2 calibration curve for the ECMS can be found in Figure 2, S4 and Supporting Information Page 2–3. Electrochemical measurements were performed using a 3-electrode setup, with a Cu disk as the

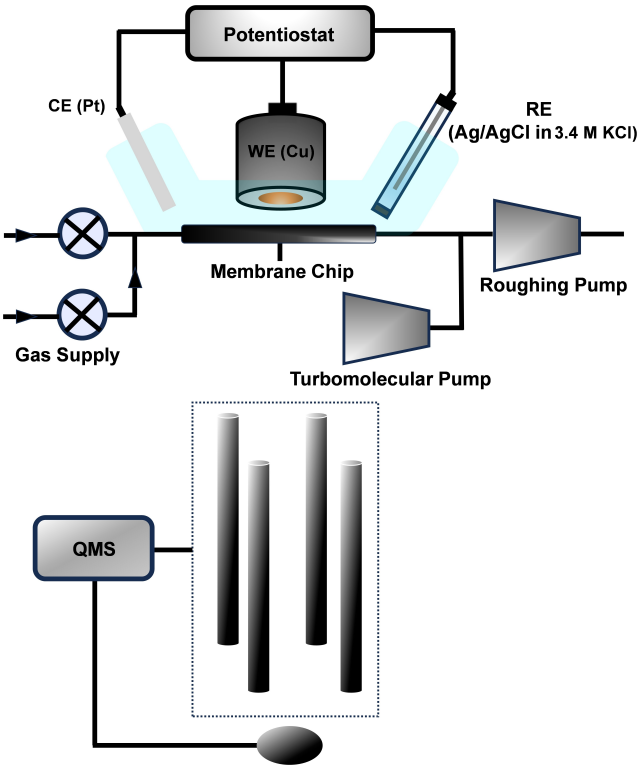

Figure 2. Schematic representation of the electrochemical mass spectrometry (ECMS) instrument. WE, RE and CE stand for working electrode, reference electrode and counter electrode respectively. QMS stands for Quadrupole Mass Spectrometer.

working electrode (with an area of approximately 0.196 cm^2), a Pt wire counter electrode, and an Ag/AgCl electrode in 3.4 M KCl solution serving as the reference electrode. In our studies, a stable Ag/AgCl reference electrode is used to ensure our understanding of the thermodynamics of the system. The choice of a Pt counter electrode rather than zinc is justified since only the reactions taking place at the copper working electrode are relevant to the present study. An electrolyte of 0.5 M $ZnSO_4$ with pH ≈4 was used for all ECMS trials. To simulate a practical coin cell cycling condition, we performed chronopotentiometry at practically relevant current densities; Figure 3(a) displays the applied current densities (−0.5, −1 and −1.5 mA/geometric cm^2: blue, red and green curves on Figure 3(a), respectively) as a function of time. Time is referenced at 0 s, which indicates the start of current application for all three cases. The current was applied for a duration of 600 s, after which no further current was applied. The WE potential remained constant at ≈0.17 V vs. Ag/AgCl for all cases before the application of current (<0 s). This potential is solely set by the $Cu^0|Zn^{2+}$ interface. The voltage response after the application of current is illustrated in Figure 3(b). The observed voltage trace closely resembles what is typically observed during the first plating cycle in an asymmetric Cu|Zn half-cell.[35,42] As anticipated, the nucleation overpotential scales with the applied current density, with values of 12 mV, 14 mV, and 16 mV for −0.5 mA/cm^2, −1 mA/cm^2, and −1.5 mA/cm^2. When the application of the current was ceased, the cell potential was measured to be near −0.82 V vs. Ag/AgCl. This potential is set by two different interfaces: $Cu^0|Zn^{2+}$ and $Zn^0|Zn^{2+}$. Along with monitoring the electrode potential as function of time, the amount of evolved hydrogen was probed as a function of time as shown in Figure 2(c). In all cases, the baseline flux of H_2 was allowed to stabilize before the application of current and has been subtracted. For a detailed explanation of the mechanism for detecting the evolved gas using ECMS, please refer to Supporting Information page no. 2, 3. The application of current results in a sharp increase in the detected H_2 in the system, which then slowly decays over time. The initial spike in H_2 may correspond to HER on the bare copper surface before significant Zn is deposited.

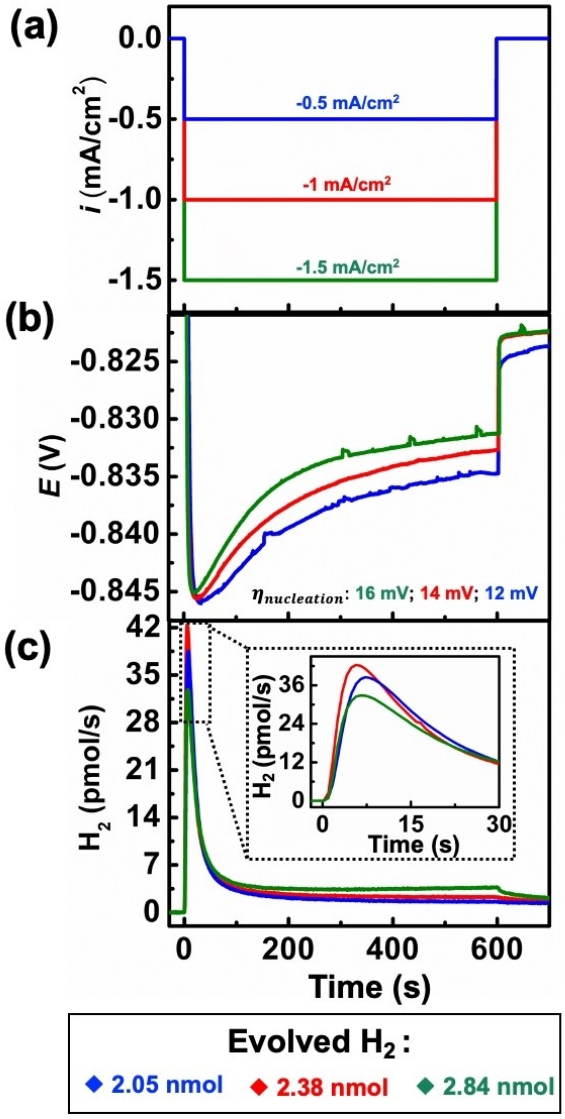

Figure 3. In situ electrochemical mass spectrometry data for the electrodeposition of Zn on Cu substrate in a three-electrode setup at three different applied current densities (−0.5, −1, and −1.5 mA/cm^2). (a) Applied current vs. time; (b) Recorded voltage (vs. Ag/AgCl in 3.4 M KCl) vs. time; (c) Real-time dynamics and quantification of evolved hydrogen vs. time.

Before delving into quantifying the amount of evolved hydrogen during the electrodeposition of zinc and calculating the faradaic efficiency for the zinc deposition, it is essential to understand a few key observations about the voltammogram presented in Figure 1(a). It is not clear from Figure 1(a) what the exact overpotential needed for HER on a Cu substrate is and why no HER is observed prior to the nucleation of zinc. To answer these questions, two independent experiments were performed involving the use of two different electrolytes: Aqueous 1 M $ZnCl_2$ and 1 M KCl in water. Linear sweep voltammetry with 1 M $ZnCl_2$ shown in Figure S5 (a) resembles the data shown in Figure 1(a), wherein a nucleation overpotential of approximately −1 V vs. Ag/AgCl (inset (i) in Figure S5(a)) was noted. The characteristic nature of the curve is also similar to Figure 1(a), where we observe an initial charge transfer followed by a transition to diffusion control and uncontrolled dendritic growth, accompanied by significant HER. In the other set of experiments where no Zn salt was used (pink curve on Figure S5(a)), and 1 M KCl was added to water to reduce the solution resistance, we observed that HER activity on the Cu substrate occurs at an overpotential of approximately −1.32 V vs. AgCl (inset (i) in Figure S5-(a)). These observations explains why no HER activity was noted in the voltammogram presented in Figure 1 prior to the nucleation of zinc on the Cu substrate, as the overpotential needed for HER on Cu is more negative compared to the nucleation overpotential of zinc electrodeposition. The overall process in the presence and absence of zinc salt is shown in Figure S5(b) and (c).

Now, To quantify the amount of hydrogen evolved during the application of current, we integrate the area under the curves presented in Figure 2(c) between 0 and 600 seconds. As expected, a higher current value leads to the liberation of more H_2 in the system (2.05 nmol, 2.38 nmol, 2.84 nmol for −0.5, −1, and −1.5 mA/cm^2, respectively). The faradaic efficiencies to hydrogen evolution calculated for these current densities are 0.62, 0.39, and 0.31 percent, with remaining charge going to zinc deposition. A closer examination during the final moments of current application (Figure S6) reveals that once the applied current is switched off, the system continues to register continuous flux of H_2 for significant periods of time. We hypothesized that this may occur due to the release of H_2 that was trapped under the porous zinc electrodeposits after the application of current. To validate these findings, we continued to track evolved H_2 well beyond the cessation of the −1.5 mA/cm^2 current application.

Figure 4(a) shows mass spectrometry data for the −1.5 mA/cm^2 trial extended beyond the 600 s current application window. As mentioned previously, the amount of liberated H_2 during the application of current was calculated to be 2.84 nmol, as indicated by the green region in Figure 4(a). Intriguingly, the system continued to register the presence of H_2 for thousands of seconds after the current was stopped. This hydrogen probably arises from two sources: At short times following the cessation of current, the MS detects H_2 which has diffused from the electrolyte layer and from microscopic bubbles of H_2 trapped in the dendritic Zn matrix. At long times, however, the nearly constant flux of H_2 observed is likely the result of metallic zinc dissolution to Zn^{2+}. Such dissolution can occur simultaneously with the HER via a continuous corrosion process that is thermodynamically favorable at this potential and pH.[43,44] These modes of hydrogen production are depicted as the regions with different color codes in Figure 4(a), corresponding to Zn-dissolution-associated and trapped/diffusion-limited H_2 respectively. Assuming that charge to HER is completely balanced by Zn corrosion, we calculate a corrosion rate of 96 pg/s. This represents a vanishingly small loss compared to the 61 μg of zinc deposited.

Additionally, it could be argued that the H_2 flux observed after 600 seconds may not originate from the porous growth. Instead, it might be attributed to the H_2 released during the final moments of the current application. To gain further insight into this process, a control experiment was conducted using a Aq. solution 1 M perchloric acid ($HClO_4$) as the electrolyte. This experiment utilized the same experimental setup, but with a platinum electrode replacing the copper working electrode to facilitate the HER. To align with comparable experimental conditions as shown in Figure 4(a), the current magnitude was fine-tuned to induce hydrogen evolution at a sustained rate akin to the zinc electrodeposition at the 600 second time point (Figure S7 and the inset). From ECMS measurements involving the use of Pt, we replaced the zinc salt-containing electrolyte with an acid-containing electrolyte (1 M $HClO_4$) without any zinc salt. This adjustment was made to enable the application of a comparable H_2 production rate, matching the observed HER in the presence of zinc salt, and facilitating the study of hydrogen release from the trapped growth. Switching to an acid-based electrolyte ensured that no zinc deposits formed on the Pt substrate, as using a zinc-containing salt would have led to zinc deposition at the applied current density. Following the cessation of the current application, we carefully recorded the decay in H_2 flux. Notably, an immediate decline in H_2 flux was observed upon terminating the current, in contrast to the zinc electro-

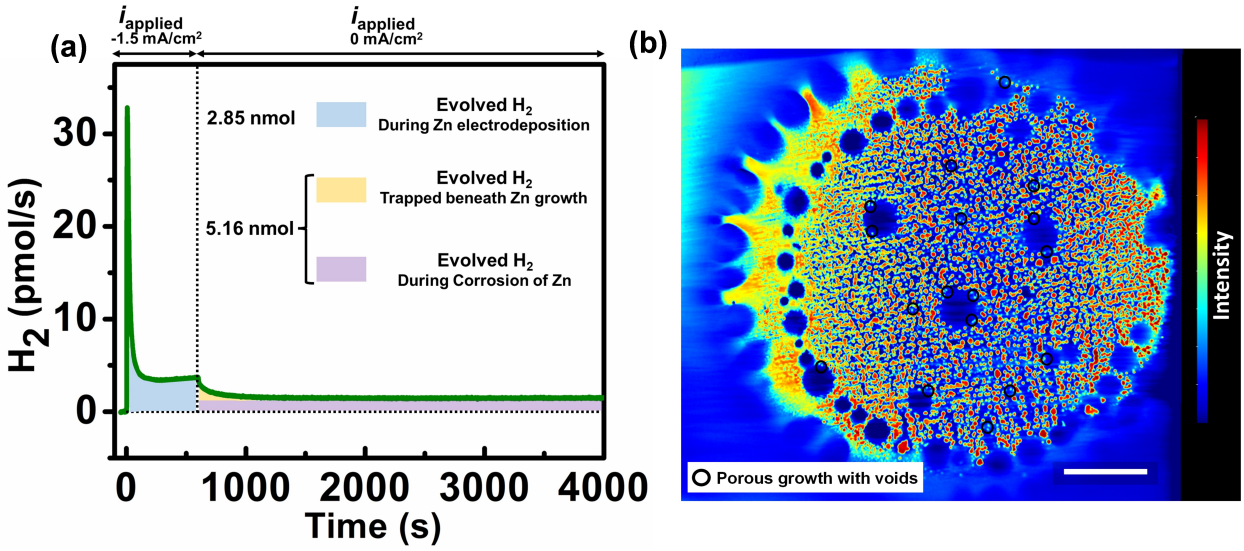

Figure 4. (a) Quantification of evolved hydrogen as a function of time, during (0 to 600 s) and after discontinuing (600 to 4000 s) the application of current (−1.5 mA/cm^2) (b) Acquired X-ray tomography image for electrodeposited zinc (-1.5 mA/cm^2 for 10 min) showing the presence of void-containing deposits. (Scale bar 3 mm). Color bar represents of the percentage abundance (intensity) of zinc; red represents the maximum concentration and blue indicates the lowest.

deposition scenario. This observation strongly indicates the existence of trapped H_2 beneath the porous electrodeposition of zinc.

The prompt decay of H_2 flux to the steady-state indicates that microstructural features of deposited Zn do not trap evolved H_2 to a significant extent. To analyse the nature of the zinc deposits, zinc was galvanostatically deposited from the same electrolyte (0.5 M $ZnSO_4$, pH ≈ 4) at the same current density and capacity (1.5 mA/cm^2 for 10 mins), and X-ray tomography of the electrode was performed. The acquired tomogram is presented in Figure 4(b), revealing the presence of voids containing zinc clusters formed as a result of the HER, as well as tiny isolated islands where no zinc clusters are present. Given the dynamic nature of the electrodeposition process involving multiple competing reactions—actual electrodeposition (Zn^{2+} to Zn^0), HER, and corrosion—the formation of isolated islands can be attributed to various factors. One possibility is the presence of a insulating passivation film, which is insulating and may hinder electrodeposition in those areas. Additionally, HER can led to bubble nucleation, and the adsorbed hydrogen bubble on the zinc substrate can block the flux of Zn^{2+} to the electrode surface. Furthermore, the adsorbed H_2 bubble typically exhibits a hemispherical geometry, where the three-phase boundary at the contact line of the bubble takes on a circular shape, resulting in isolated circle-like islands on the electrode surface. The color bar serves as a visual representation of the percentage abundance (intensity) of zinc, with red representing the maximum concentration and blue indicating the lowest.

Overall, the methodology outlined in this study offers significant benefits for two key reasons. First, it enables us to determine the faradaic efficiency of zinc electrodeposition, which is being reported for the first time. This allows us to deconvolute the total charge passed into its constituent components, which are the contributions from two distinct reduction reactions: the conversion of Zn^{2+} to Zn^0 clusters and H^+ to evolved H_2. For instance, the faradaic efficiency for the data shown in Figure 4(a) was found to be 99.7 % for Zn electrodeposition between 0 and 600 s (see Supporting Information Pg. no. 3 for the detailed calculation). It is essential to note that our efficiency calculation is based on the assumption that the total charge is solely attributed to the HER and zinc electrodeposition. Other factors, such as electron transfer-driven solvent decomposition on the electrode surface, passivation or corrosion is not considered. Secondly, the generality of the ECMS method enables convenient screening of electrolyte additives, electrolyte salts, and current collector modifications, with the goal of improving the long-term cyclability of AZMBs and suppressing the HER.

Conclusion

In summary, our study introduces an innovative in situ electrochemical mass spectrometry method for precise quantification of hydrogen evolution reactions during zinc electrodeposition. Through chronopotentiometry techniques, we examined the galvanostatic deposition of zinc at varying current densities, quantifying both potential and evolved hydrogen as a function of time. Our results showed that the magnitude of hydrogen evolution is positively correlated to applied current density. Additionally, our ECMS measurements allowed us to replicate zinc electrodeposition on a practical level, imitating coin cell conditions and offering insights into the dynamics of hydrogen evolution in real systems. In addition to hydrogen produced during the application of current, we also observed H_2 production at zero net current from the corrosion of deposited zinc. This methodology not only assesses Faradaic efficiency, distinguishing contributions from zinc electrodeposition and HER, but also provides a platform to assess the impact of electrolyte additives and modifications on enhancing the performance of advanced zinc-based metal batteries. These findings hold the promise of significantly advancing electrochemical energy storage and enhancing zinc-based battery technology and related applications.

Supporting Information

Supporting Information available.

Acknowledgements

All authors show no conflict of interest and have agreed to the final version of the manuscript. J.E.D. acknowledges Purdue University, the Sloan Foundation, and the National Science Foundation under grant CHE-2045672. B.M.T. acknowledges funding support from Purdue University. The authors acknowledge Alexandra Clark who acquired the images of cycled electrodes for this paper on a Zeiss Xradia 510 Versa 3D X-ray Microscope that was supported by the EVPRP Major Multi-User Equipment Program 2017 at Purdue University.

Conflict of Interest

The authors declare no conflict of interest.

Data Availability Statement

The data that support the findings of this study are available from the corresponding author upon reasonable request.

Keywords: Electrochemical Mass Spectrometry · Hydrogen Evolution Reaction · In-Situ Electrochemistry · Zinc Metal Battery

[1] G. Zampardi, F. La Mantia, *Nat. Commun.* **2022**, *13*, 687.
[2] J. Shin, J. Lee, Y. Park, J. W. Choi, *Chem. Sci.* **2020**, *1*, 2028–2044.

[3] C. Nie, G. Wang, D. Wang, M. Wang, X. Gao, Z. Bai, N. Wang, J. Yang, Z. Xing, S. Dou, *Adv. Energy Mater.* **2023**, *13*, 2300606.
[4] L. Miao, Z. Guo, L. Jiao, *Energy Mater.* **2023**, *3*, 300014.
[5] F. Wan, X. Zhou, Y. Lu, Z. Niu, J. Chen, *ACS Energy Lett.* **2020**, *5*, 3569–3590.
[6] S. Liu, R. Zhang, J. Mao, Y. Zhao, Q. Cai, Z. Guo, *Sci. Adv.* **2022**, *8*, eabn5097.
[7] H. Li, S. Guo, H. Zhou, *Energy Storage Mater.* **2023**, *56*, 227–257.
[8] B. Tang, L. Shan, S. Liang, J. Zhou, *Energy Environ. Sci.* **2019**, *2*, 3288–3304.
[9] L. Yuan, J. Hao, C. C. Kao, C. Wu, H. K. Liu, S. X. Dou, S. Z. Qiao, *Energy Environ. Sci.* **2021**, *4*, 5669–5689.
[10] W. Du, E. H. Ang, Y. Yang, Y. Zhang, M. Ye, C. C. Li, *Energy Environ. Sci.* **2020**, *3*, 3330–3360.
[11] W. Lu, C. Zhang, H. Zhang, X. Li, *ACS Energy Lett.* **2021**, *6*, 2765–2785.
[12] J. Yang, B. Yin, Y. Sun, H. Pan, W. Sun, B. Jia, S. Zhang, T. Ma, *Nano-Micro Lett.* **2022**, *14*, 42.
[13] X. Yu, Z. Li, X. Wu, H. Zhang, Q. Zhao, H. Liang, H. Wang, D. Chao, F. Wang, Y. Qiao, H. Zhou, S. G. Sun, *Joule* **2023**, *7*, 1145–1175.
[14] X. Guo, G. He, *J. Mater. Chem. A* **2023**, 11987–12001.
[15] J. Wang, Y. Yang, Y. Zhang, Y. Li, R. Sun, Z. Wang, H. Wang, *Energy Storage Mater.* **2023**, *35*, 19–46.
[16] J. Chen, W. Zhao, J. Jiang, X. Zhao, S. Zheng, Z. Pan, X. Yang, *Energy Storage Mater.* **2023**, *59*, 102767.
[17] W. Zhang, G. He, *Angew. Chem. Int. Ed.* **2023**, *62*, e202218466.
[18] M. R. Shaik, S. M. Olidan, J. Kim, K. Y. Cho, S. Yoon, *J. Mater. Chem. A* **2023**, *1*, 6403–6412.
[19] W. Yuan, X. Nie, G. Ma, M. Liu, Y. Wang, S. Shen, N. Zhang, *Angew. Chem. Int. Ed.* **2023**, *62*, e202218386.
[20] T. Ling, T. Zhang, B. Ge, L. Han, L. Zheng, F. Lin, Z. Xu, W. Bin Hu, X. W. Du, K. Davey, S. Z. Qiao, *Adv. Mater.* **2019**, *31*, 1807771.
[21] Z. Yi, G. Chen, F. Hou, L. Wang, J. Liang, *Adv. Energy Mater.* **2021**, *11*, 2003065.
[22] H. Wang, H. Li, Y. Tang, Z. Xu, K. Wang, Q. Li, B. He, Y. Liu, M. Ge, S. Chen, T. Hao, G. Xing, Y. Zhang, *Adv. Funct. Mater.* **2022**, *32*, 2207898.
[23] W. Guo, X. Bai, Z. Cong, C. Pan, L. Wang, L. Li, C. Chang, W. Hu, X. Pu, *ACS Appl. Mater. Interfaces* **2022**, 41988–41996.
[24] K. Zhao, G. Fan, J. Liu, F. Liu, J. Li, X. Zhou, Y. Ni, M. Yu, Y. M. Zhang, H. Su, Q. Liu, F. Cheng, *J. Am. Chem. Soc.* **2022**, *1*, 11129–11137.
[25] Q. Zhang, Y. Ma, Y. Lu, Y. Ni, L. Lin, Z. Hao, Z. Yan, Q. Zhao, J. Chen, *J. Am. Chem. Soc.* **2022**, *1*, 18435–18443.
[26] B. Niu, Z. Li, D. Luo, X. Ma, Q. Yang, Y. E. Liu, X. Yu, X. He, Y. Qiao, X. Wang, *Energy Environ. Sci.* **2023**, *6*, 1662–1675.
[27] Z. Liu, R. Wang, Q. Ma, J. Wan, S. Zhang, L. Zhang, H. Li, Q. Luo, J. Wu, T. Zhou, J. Mao, L. Zhang, C. Zhang, Z. Guo, *Adv. Funct. Mater.* **2023**, https://doi.org/10.1002/adfm.202214538.
[28] M. Yan, N. Dong, X. Zhao, Y. Sun, H. Pan, *ACS Energy Lett.* **2021**, *6*, 3236–3243.
[29] F. Wang, O. Borodin, T. Gao, X. Fan, W. Sun, F. Han, A. Faraone, J. A. Dura, K. Xu, C. Wang, *Nat. Mater.* **2018**, *17*, 543–549.
[30] J. Xie, Z. Liang, Y. C. Lu, *Nat. Mater.* **2020**, *9*, 1006–1011.
[31] C. C. Kao, C. Ye, J. Hao, J. Shan, H. Li, S. Z. Qiao, *ACS Nano* **2023**, *7*, 3948–3957.
[32] Z. Chen, C. Li, Q. Yang, D. Wang, X. Li, Z. Huang, G. Liang, A. Chen, C. Zhi, *Adv. Mater.* **2021**, *33*, 2105426.
[33] L. Ma, Q. Li, Y. Ying, F. Ma, S. Chen, Y. Li, H. Huang, C. Zhi, *Adv. Mater.* **2021**, *33*, 2007406.
[34] D. B. Trimarco, S. B. Scott, A. H. Thilsted, J. Y. Pan, T. Pedersen, O. Hansen, I. Chorkendorff, P. C. K. Vesborg, *Electrochim. Acta* **2018**, *68*, 520–530.
[35] L. Cao, D. Li, E. Hu, J. Xu, T. Deng, L. Ma, Y. Wang, X. Q. Yang, C. Wang, *J. Am. Chem. Soc.* **2020**, *1*, 21404–21409.
[36] P. Bai, J. Li, F. R. Brushett, M. Z. Bazant, *Energy Environ. Sci.* **2016**, *9*, 3221–3229.
[37] R. N. Wasalathanthri, R. Akolkar, *J. Electrochem. Soc.* **2022**, *169*, 092519.
[38] W. Du, Z. Zhang, F. Iacoviello, S. Zhou, R. E. Owen, R. Jervis, D. J. L. Brett, P. R. Shearing, *ACS Appl. Mater. Interfaces* **2022**, 14196–14205.
[39] Q. Li, A. Chen, D. Wang, Y. Zhao, X. Wang, X. Jin, B. Xiong, C. Zhi, *Nat. Commun.* **2022**, *13*, 3699.
[40] S. D. Pu, B. Hu, Z. Li, Y. Yuan, C. Gong, Z. Ning, C. Chau, S. Yang, S. Zhang, L. Pi, Y. T. Tang, J. Yue, T. J. Marrow, X. Gao, P. G. Bruce, A. W. Robertson, *Joule* **2023**, *7*, 366–379.
[41] H. J. Kim, S. Kim, K. Heo, J. H. Lim, H. Yashiro, S. T. Myung, *Adv. Energy Mater.* **2023**, *13*, 2203189.
[42] K. Zhao, F. Liu, G. Fan, J. Liu, M. Yu, Z. Yan, N. Zhang, F. Cheng, *ACS Appl. Mater. Interfaces* **2021**, 47650–47658.
[43] B. Beverskog, I. Puigdomenech, *Corros. Sci.* **1997**, *39*, 107–114.
[44] K. Wippermann, J. W. Schultze, R. Kessel, J. Penninger, H. Kgaa, F. R. G. Dfisseldorf, *Corros. Sci.* **1991**, *32*, 205–223.
[45] Z. Wang, J. Diao, J. N. Burrow, Z. W. Brotherton, N. A. Lynd, G. Henkelman, C. B. Mullins, *Adv. Funct. Mater.* **2023**, https://doi.org/10.1002/adfm.202311271.
[46] Z. Wang, J. Diao, J. N. Burrow, K. K. Reimund, N. Katyal, G. Henkelman, C. B. Mullins, *Adv. Funct. Mater.* **2023**, *33*, 2304791.
[47] Z. Wang, J. Diao, K. Kawashima, J. A. Weeks, R. R. Vaidyula, R. A. Marquez, N. Miller, G. Henkelman, C. B. Mullins, *J. Mater. Chem. A* **2023**, *11*, 18881.

Manuscript received: December 10, 2023
Accepted manuscript online: January 2, 2024
Version of record online: ■■, ■■

Research Articles

Zinc Batteries

K. Roy, A. Rana, J. N. Heil, B. M. Tackett,*
J. E. Dick* **e202319010**

For Zinc Metal Batteries, How Many Electrons go to Hydrogen Evolution? An Electrochemical Mass Spectrometry Study

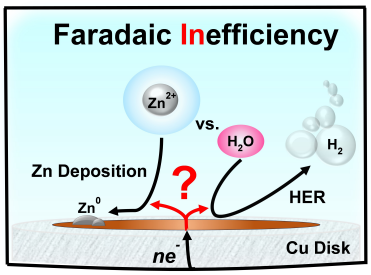

This study introduces an innovative in situ electrochemical mass spectrometry method for precise quantification of hydrogen evolution reactions during zinc electrodeposition. The results show that the magnitude of hydrogen evolution is positively correlated to applied current density.